J|A|C|S
ARTICLES
Published on Web 11/27/2003

Transfer of π-Conjugated Columnar Stacks from Solution to Surfaces

Pascal Jonkheijm, Freek J. M. Hoeben, Ralf Kleppinger, Jeroen van Herrikhuyzen, Albertus P. H. J. Schenning,* and E. W. Meijer*

Contribution from the Laboratory of Macromolecular and Organic Chemistry, Eindhoven University of Technology, P.O. Box 513, 5600 MB Eindhoven, The Netherlands

Received September 3, 2003; E-mail: j.schenning@tue.nl; e.w.meijer@tue.nl

Abstract: Three hydrogen-bonded oligo(*p*-phenylenevinylene)s, **OPV3**, **OPV4**, and **OPV5**, that differ in conjugation length have been synthesized and fully characterized. All three compounds contain chiral side chains, long aliphatic chains, and a ureido-*s*-triazine hydrogen bonding unit. ^{1}H NMR and photophysical measurements show that the OPV oligomers grow hierarchically in an apolar solvent; initially, dimers are formed by hydrogen bonds that subsequently develop into stacks by $\pi-\pi$ interactions of the phenylenevinylene backbone with induced helicity via the chiral side chains. SANS measurements show that rigid cylindrical objects are formed. Stacks of **OPV4** have a persistence length of 150 nm and a diameter of 6 nm. **OPV3** shows rigid columnar domains of 60 nm with a diameter of 5 nm. Temperature and concentration variable measurements show that the stability of the stacks increases with the conjugation length as a result of more favorable $\pi-\pi$ interactions. The transfer of the single cylinders from solution to a solid support as isolated objects is only possible when specific concentrations and specific solid supports are used as investigated by AFM. At higher concentrations, an intertwined network is formed, while, at low concentration, ill-defined globular objects are observed. Only in the case of inert substrates (graphite and silicium oxide) single fibers are visible. In the case of the repulsive surfaces (mica and glass), clustering of the stacks occurs, while, at attractive surfaces (gold), the stacks are destroyed.

Introduction

Noncovalent interactions of molecular building blocks into supramolecular structures is a fundamental building principle for biological materials and found in various systems ranging from double stranded DNA to complex structures such as Tobacco Mosaic Virus.[1] The appeal that nature holds lies in the fact that the information at the molecular level guides the organization at the supramolecular level. This intelligent engineering of molecules has inspired many research groups to direct disordered molecules via molecular recognition into well-organized self-assembled structures with a specific function.[2] A manifold of examples exist in which different types of noncovalent interactions are applied to construct complex architectures adopting stable and compact conformations which may find applications in the field of biology and materials science.[3] An emerging challenge for applying these supramolecular architectures is the often required nanomanipulation of the objects. A restricted number of studies show the opportunities and limitations of transferring the objects from solution to surfaces in a controlled way.[4]

In optoelectronic materials science, the specific properties of a device are likewise determined by the chemical structure and the supramolecular organization of the building blocks. Although the control of the chemical composition is thoroughly investigated, ways to control the supramolecular organization are deficient. The supramolecular organization is mainly investigated in solution, while the organization in the solid state as relevant to devices is almost unknown. Columnar liquid crystalline materials as bulk materials have a high degree of organization in the solid state, and high electron and hole mobility have already been reported.[5] Very recently, Percec et

(1) Klug, A. *Angew. Chem.* **1983**, *95*, 579−596.
(2) For reviews, see: (a) Brunsveld, L.; Folmer, B. J. B.; Meijer, E. W.; Sijbesma, R. P. *Chem. Rev.* **2001**, *101*, 4071−4097. (b) Prins, L. J.; Reinhoudt, D. N.; Timmerman, P. *Angew. Chem., Int. Ed.* **2001**, *40*, 2382−2426. (c) Sherrington, D. C.; Taskinen, K. A. *Chem. Soc. Rev.* **2001**, *30*, 83. (d) Bong, D. T.; Clark, T. D.; Granja, J. R.; Ghadiri, M. R. *Angew. Chem., Int. Ed.* **2001**, *40*, 988−1011. (e) Ciferri, A. *Macromol. Rapid Commun.* **2002**, *23*, 511−529. (f) Hartgerink, J. D.; Zubarev, E. R.; Stupp, S. I. *Curr. Opin. Solid State Mater. Sci.* **2001**, *5*, 355−361.
(3) For examples, see: (a) Pralle, M. U.; Whitaker, C. M.; Braun, P. V.; Stupp, S. I. *Macromolecules* **2000**, *33*, 3550−3556. (b) Klok, H.-A.; Jolliffe, K. A.; Schauer, C. L.; Prins, L. J.; Spatz, J. P.; Möller, M.; Timmerman, P.; Reinhoudt, D. N. *J. Am. Chem. Soc.* **1999**, *121*, 7154−7155. (c) Zerowski, J. A.; Seto, C. T.; Wierda, D. A.; Whitesides, G. M. *J. Am. Chem. Soc.* **1990**, *112*, 9025−9026. (d) Gottarelli, G.; Mezzina, E.; Spada, G. P.; Carsughi, F.; di Nicola G.; Mariani, P.; Sabaticci, A.; Bonazzi, S. *Helv. Chim. Acta* **1996**, *79*, 220−234. (e) Mio, M. J.; Prince, R. B.; Moore, J. S.; Kuebel, C.; Martin, D. C. *J. Am. Chem. Soc.* **2000**, *122*, 6134−6135. (f) Percec, V.; Ahn, C.-H.; Ungar, G.; Yeardley, D. J. P.; Möller, M.; Sheiko, S. S. *Nature* **1998**, *391*, 161−164. (g) Hirschberg, J. H. K. K.; Brunsveld, L.; Ramzi, A.; Vekemans, J. A. J. M.; Sijbesma, R. P.; Meijer, E. W. *Nature* **2000**, *407*, 167−170.
(4) For examples, see: (a) Rapaport, H.; Kim, H. S.; Kjaer, K.; Howes, P. B.; Cohen, S.; Als-Nielsen, J.; Ghadiri, M. R.; Leiserowitz, L.; Lahav, M. *J. Am. Chem. Soc.* **1999**, *121*, 1186−1191. (b) van Gorp, J. J.; Vekemans, J. A. J. M.; Meijer, E. W. *J. Am. Chem. Soc.* **2002**, *124*, 14759−14769. (c) Fenniri, H.; Deng, B.-L.; Ribbe, A. E. *J. Am. Chem. Soc.* **2002**, *124*, 11064−11072. (d) Zubarev, E. R.; Pralle, M. U.; Sone, E. D.; Stupp, S. I. *J. Am. Chem. Soc.* **2001**, *123*, 4105−4106. (e) Schönherr, H.; Paraschiv, V.; Zapotoczny, S.; Crego-Calama, M.; Timmerman, P.; Frank, C. W.; Vancso, G. J.; Reinhoudt, D. N. *Proc. Natl. Acad. Sci. U.S.A.* **2002**, *99*, 5025−5027. (f) Kawasaki, T.; Tokuhiro, M.; Kimizuka, N.; Kunitake, T. *J. Am. Chem. Soc.* **2001**, *123*, 6792−6800.

Chart 1. Molecular Structures of **OPV3**, **OPV4**, and **OPV5** as Calculated by Molecular Dynamics and Subsequent Energy Minimization at 300 K for 50 ps[a]

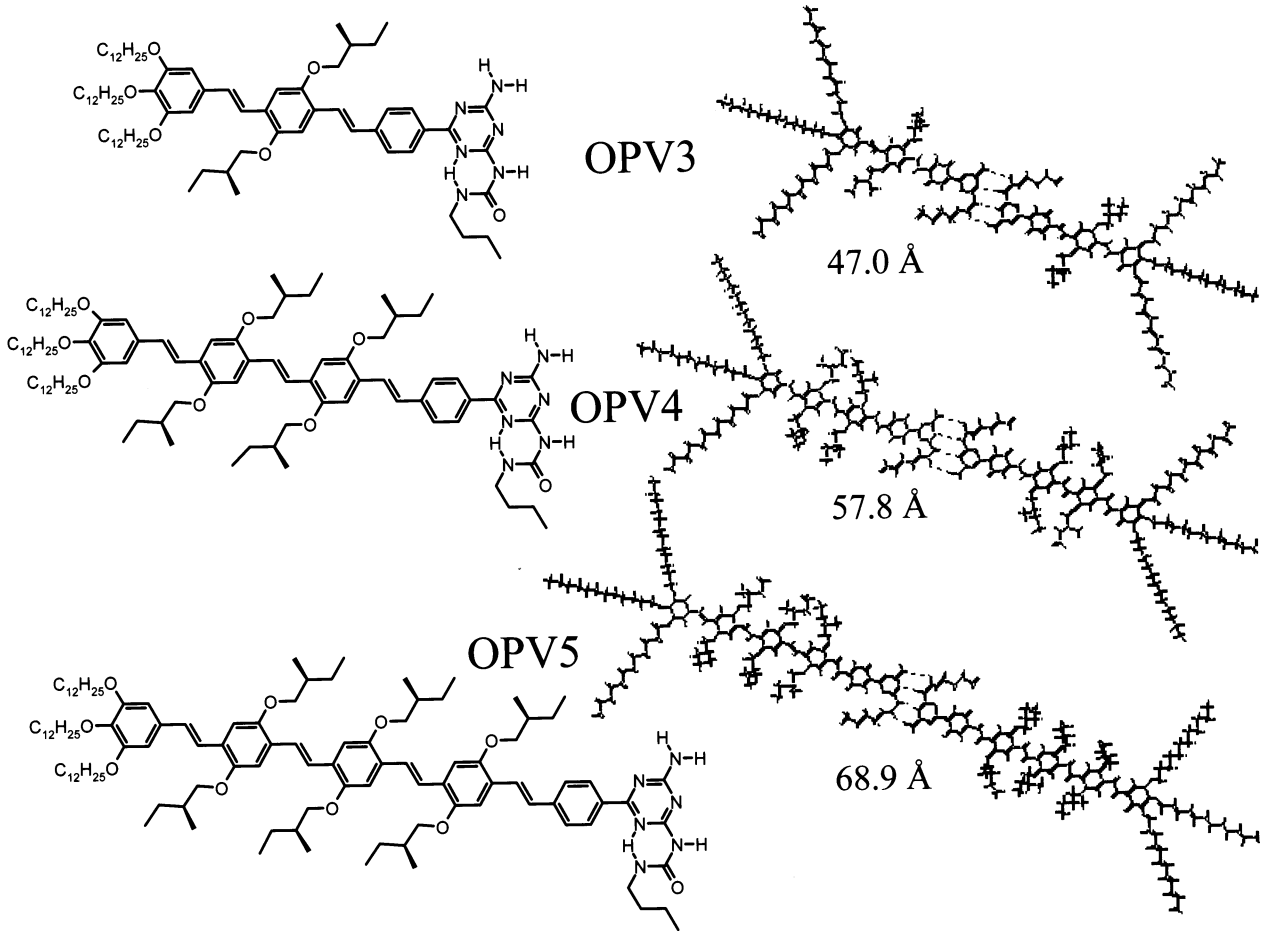

[a] Indicated lengths are from the conjugated dimers omitting the dodecyloxy tails.

al. presented a supramolecular strategy to program electroactive organic molecules into liquid crystalline columns that display high mobility using numerous concepts of supramolecular chemistry.[6]

The solid-state organization of organic molecules at the nanometer level will also be crucial for the ongoing miniaturization of electro-optical devices. Such assemblies could be an alternative for (hybrid) inorganic wires,[7] carbon nanotubes,[8] and organic molecules[9] as a nanosized device. Numerous examples of self-assembled semiconducting organic rods in solution have already been presented in recent literature;[10] however, the behavior of such nanofibers on a solid support are scarce and yet to be exploited. Therefore, the understanding of the parameters that play a role in the transfer process of self-assembled molecules from solution to a solid support will be of great importance.

Recently we reported on the hierarchical formation of chiral stacks based on a semiconducting chiral tetra(*p*-phenylenevinylene) functionalized with a quadruple ureido-*s*-triazine hydrogen bonding unit (**OPV4**, Chart 1).[10b] As shown by ^{1}H NMR and photophysical studies, monomers and hydrogen bonded dimers are present at room temperature in chloroform, while, in dodecane, helical stacks are formed. We now present a comprehensive study on this hierarchical organization using three different oligo(*p*-phenylenevinylene) (**OPV**) units equipped with a hydrogen bonding unit (Chart 1) showing the influence of the conjugation length on the stability of the stacks. Furthermore, the shape of the aggregates in solution was studied by small-angle neutron scattering (SANS). Additionally, the

(5) (a) Van der Craats, A. M.; Warman, J. M.; Fechtenkötter, A.; Brand, J. D.; Harbison, M. A.; Müllen, K. *Adv. Mater.* **1999**, *11*, 1469−1472. (b) Schmidt-Mende, L.; Fechtenkötter, A.; Müllen, K.; Moons, E.; Friend, R. H.; MacKenzie, J. D. *Science* **2001**, *293*, 1119−1122.
(6) Percec, V.; Glodde, M.; Bera, T. K.; Mlura, Y.; Shlyanovskaya, I.; Singer, K. D.; Balagurusamy, V. S. K.; Helney, P. A.; Schnell, I.; Rapp, A.; Spiess, H.-W.; Hudson, S. D.; Duan, H. *Nature* **2002**, *417*, 384−387.
(7) (a) Sone, E. D.; Zubarev, E. R.; Stupp, S. I. *Angew. Chem., Int. Ed.* **2002**, *41*, 1705−1709. (b) Duan, X.; Huang, Y.; Cui, Y.; Wang, J.; Lieber, C. M. *Nature* **2001**, *409*, 66−69. (c) Huang, Y.; Duan, X.; Cui, Y.; Lauhon, L. J.; Kim, K.-H.; Lieber, C. M. *Science* **2001**, *294*, 1313−1317.
(8) (a) Bachtold, A.; Hadley, P.; Nakanishi, T.; Dekker, C. *Science* **2001**, *294*, 1317−1320. (b) Postma, H. W. Ch.; Teepen, T.; Yao, Z.; Grifoni, M.; Dekker, C. *Science* **2001**, *293*, 76−79.
(9) (a) Tseng, G. Y.; Ellenbogen, J. C. *Science* **2001**, *294*, 1293−1294. (b) Chen, J.; Reed, M. A.; Rawlett, A. M.; Tour, J. M. *Science* **1999**, *286*, 1550−1552. (c) Gorman, C. B.; Carroll, R. L. *Angew. Chem., Int. Ed.* **2002**, *41*, 4378−4400.
(10) (a) Schenning, A. P. H. J.; van Herrikhuyzen, J.; Jonkheijm, P.; Chen, Z.; Würthner, F.; Meijer, E. W. *J. Am. Chem. Soc.* **2002**, *124*, 10252−10253. (b) Schenning, A. P. H. J.; Jonkheijm, P.; Peeters, E.; Meijer, E. W. *J. Am. Chem. Soc.* **2001**, *123*, 409−416. (c) Engelkamp, H.; Middelbeek, S.; Nolte, R. J. M. *Nature* **1999**, *284*, 785. (d) Schenning, A. P. H. J.; Kilbinger, A. F. M.; Biscarini, F.; Cavellini, M.; Cooper, H. J.; Derrick, P. J.; Feast, W. J.; Lazzaroni, R.; Leclère, Ph.; McDonnell, L. A.; Meijer, E. W.; Meskers, S. C. J. *J. Am. Chem. Soc.* **2002**, *124*, 1269−1275. (e) Schoonbeek, F. S.; van Esch, J. H.; Wegewijs, B.; Rep, D. B. A.; de Haas, M. P.; Klapwijk, T. M.; Kellog, R. M.; Feringa, B. L. *Angew. Chem., Int. Ed.* **1999**, *38*, 1393−1397. (f) Würthner, F.; Thalacker, C.; Sautter, A. *Adv. Mater.* **1999**, *11*, 754−758. (g) Ajayaghosh, A.; George, S. J. *J. Am. Chem. Soc.* **2001**, *123*, 5148−5149. (h) Apperloo, J. J.; Janssen, R. A. J.; Malenfant, P. R. L.; Fréchet, J. M. J. *Macromolecules*, **2000**, *33*, 7038−7043.

Chart 2. Synthetic Route toward Quadruple Hydrogen Bonding Motif Functionalized **OPV*n***, Respectively (*n* = Number of Phenylenevinylene Units)[a]

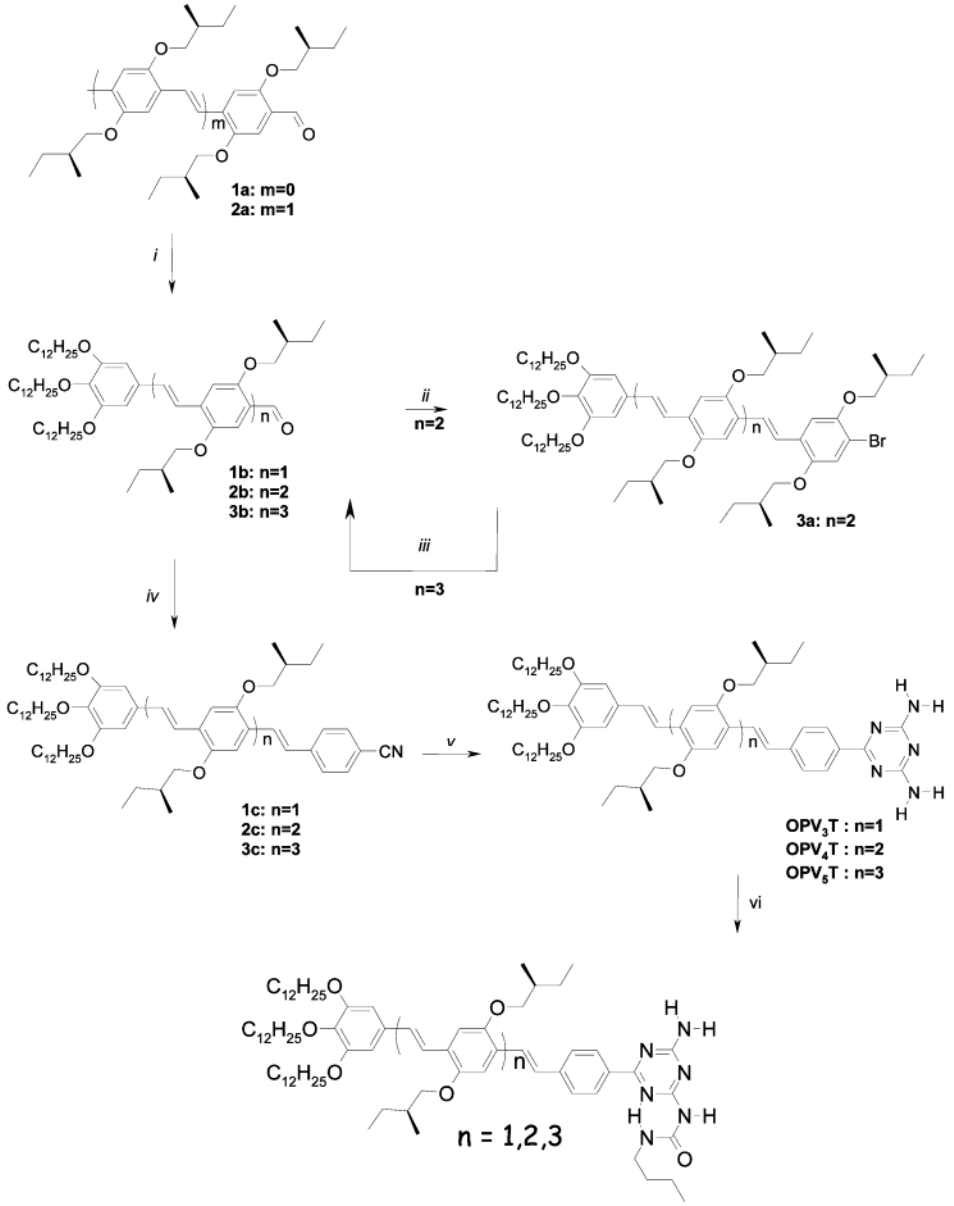

[a] (*i*) (a) Methanol, trimethylorthoformate, amberlite; (b) (*E*)-*N*-Phenyl-3,4,5-tridodecyloxybenzaldimine, potassium *tert*-butyloxide, DMF. (*ii*) Diethyl(4-bromobenzyl)phosphonate, potassium *tert*-butyloxide, DMF. (*iii*) *n*-Butyllithium, DMF, diethyl ether. (*iv*) Diethyl(4-cyanobenzyl)phosphonate, potassium *tert*-butyloxide, DMF. (*v*) Dicyanediamide, 2-methoxyethanol, potassium hydroxide. (*vi*) *n*-Butylisocyanate, pyridine.

supramolecular organization of these stacks on different types of solid supports was studied with atomic force microscopy (AFM).

Results and Discussion

Synthesis. The synthesis of the ureido-*s*-triazine hydrogen bond substituted **OPV** oligomers **OPV5** and **OPV3** is based on the synthetic route previously described for tetramer **OPV4** (Chart 2).[10b] Pentamer **OPV5** was obtained by an additional cycle with respect to **OPV4** (steps *ii* and *iii*) of Wittig−Horner and Bouveault reactions to elongate the conjugation length.[10b] The synthesis of trimer **OPV3** was shortened by such a cycle. Analytically pure materials were obtained after extensive purification procedures. The ^{1}H NMR and ^{13}C NMR spectra of **OPV4T** were completely assigned with help of 1D and 2D NMR techniques and used as a reference for the other compounds (see the Supporting Information). The final products were fully characterized by ^{1}H NMR, ^{13}C NMR, MALDI-TOF, and elemental analysis. ^{1}H NMR spectra in chloroform of the ureido-*s*-triazine substituted **OPV** oligomers showed low field NH resonances at $\delta = 10.3$, 9.9, and 9.3 ppm indicating the presence of monomers and hydrogen bonded dimers. Previously, we found an association constant of 2×10^4 M^{-1} for both **OPV4** and a ureido-*s*-triazine derivate lacking the **OPV** moiety.[10b] Therefore, we propose that the dimerization constant is similar for all **OPV** oligomers.

Photophysics in Solution. UV−vis and fluorescence spectroscopies were performed on chloroform solutions of **OPV3**, **OPV4**, and **OPV5** showing clearly the effect of conjugation length. A red shift of the absorption maximum ($\lambda = 412$, 437,

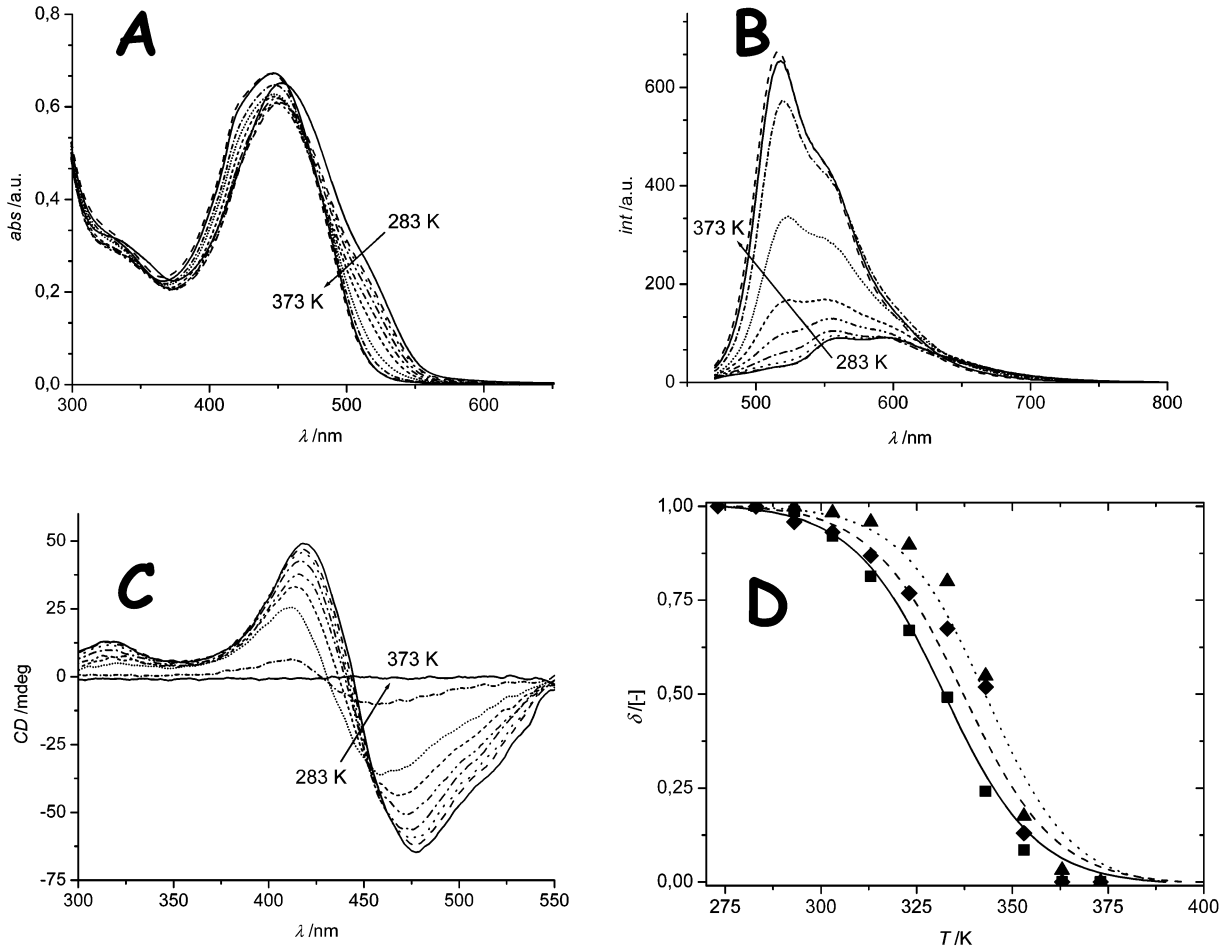

Figure 1. Variable temperature UV−vis spectra (A), fluorescence (B), and CD (C) spectra of **OPV5** (dodecane, 4×10^{-5} M). The coinciding melting transition curves are plotted as aggregated fraction (ϕ) versus temperature (normalized data points from CD (◆), UV−vis (■), and fluorescence (▲) spectra).

Table 1. Absorption Maxima, Emission Maxima (Excited at λ_{max} at $T = 293$ K) and the Anisotropy Factor of Adsorption (g_{abs}) of **OPV*n*** in Chloroform and Dodecane, Media in Which the Molecules Are Molecularly Dissolved and Aggregated, Respectively[a]

	UV/vis (λ_{max} in nm)		PL ($\lambda_{em,max}$ in nm)		CD (g_{abs})	ΔH	ΔS
	$CHCl_3$	dodecane	$CHCl_3$	dodecane	dodecane	(kJ mol^{-1})	(J mol^{-1} K^{-1})
OPV3	412	411	470	478, 508	1.12×10^{-3}	−129.3	−334.9
OPV4	437	440	501	525, 550	1.89×10^{-3}	−161.4	−399.5
OPV5	444	453	515	561, 595	2.06×10^{-3}	−168.4	−405.7

[a] The enthalpy and entropy values as obtained from the van 't Hoff plot representation of the melting transition temperatures.

and 444 nm, respectively) and emission maximum (λ = 470, 501, and 515 nm, respectively) was observed upon going from **OPV3** to **OPV4** to **OPV5** (Table 1). The observed $\pi-\pi^*$ transitions are similar to related oligo(*p*-phenylenevinylene)s.[11]

The UV−vis and fluorescence spectra of a heated (343 K) apolar dodecane solution of **OPV5** were comparable to those in chloroform indicating molecularly dissolved monomeric and hydrogen bonded dimeric species.[11] As previously found for **OPV4**, lowering of the temperature resulted similarly in a shoulder at the red side of the absorption maximum (Figure 1A) while simultaneously the fluorescence intensity decreased and shifted to the red indicating aggregation (Figure 1B, Table 1). Moreover, at the $\pi-\pi^*$ transition, a bisignated Cotton effect in the circular dichroism (CD) spectrum was observed having a negative exciton coupling (Figure 1C). This negative coupling suggests the presence of a left-handed helical arrangement of the transition dipoles of the **OPV** molecules.[12] All spectral characteristics are red shifted with respect to **OPV4** as a result of the elongated π-system (Table 1). Upon increasing the temperature, we observed that spectral change in the CD spectrum for **OPV5** occurred accompanied with changes in the UV−vis and fluorescence spectra. When the fraction of aggregated species (ϕ) versus the temperature (T) is plotted for the three different photophysical techniques, fairly equivalent transition curves are obtained (Figure 1D). The melting of the stacks takes place in a relatively narrow temperature range indicating that the thermal denaturation of the stacks is a highly cooperative process. Probably the stability of the stacks is the consequence of many reinforcing bonds, each of which is relatively weak. The formation of any of these stabilizing bonds very much depends on whether adjacent bonds are also made. The abruptness of the transition reveals that OPV stacks are stabilized by cooperative interactions such as in DNA and collagen.[13]

Analogous temperature-dependent spectral transformations were observed for **OPV3** (Figure 2). The absorption and

(11) Peeters, E.; Marcos, A.; Meskers, S. C. J.; Janssen, R. A. J. *J. Chem. Phys.* **2000**, *112*, 9445−9454.

(12) Davydov, A. S. *Zh. Eksp. Teor. Fiz.* **1948**, *18*, 210−218.

(13) Stryer, L. In *Biochemistry*, 3rd ed.; W. H. Freeman and Company: New York, 1975.

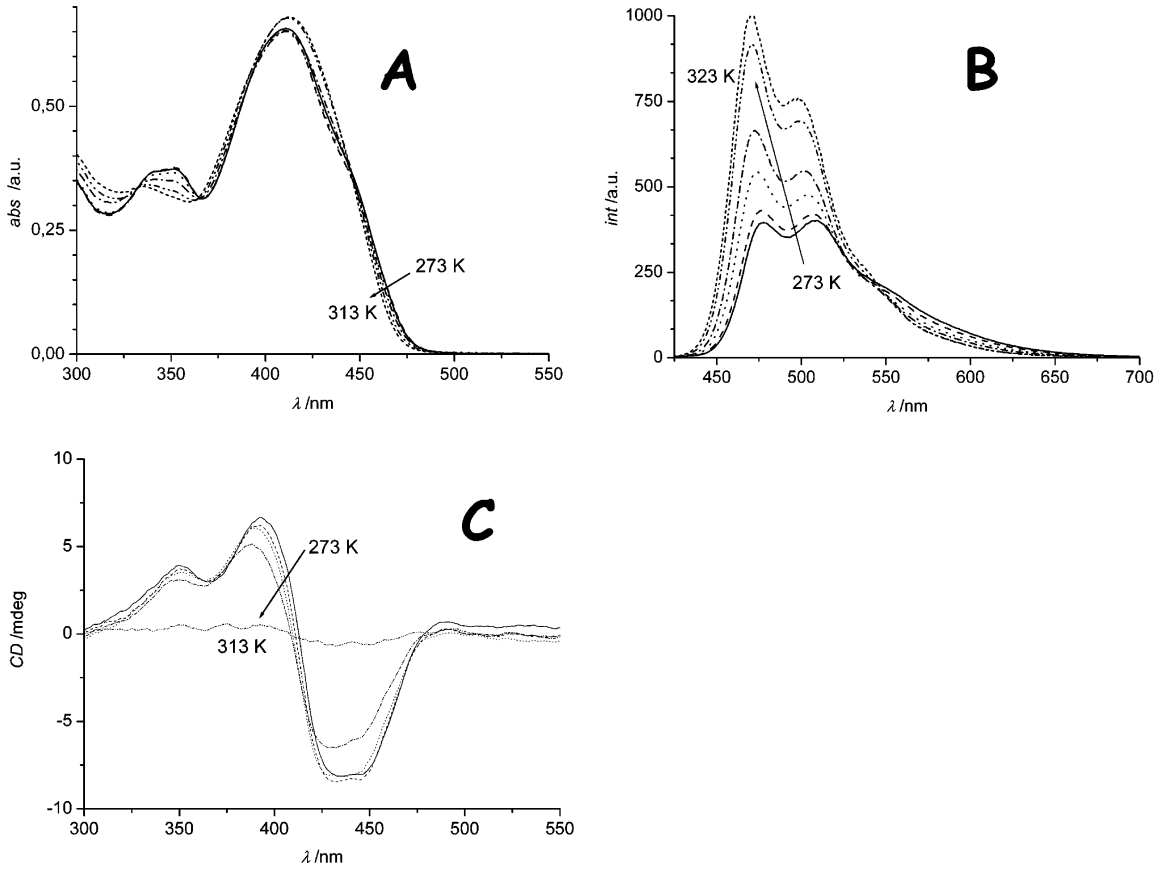

Figure 2. Variable temperature UV−vis (A), fluorescence (B), and CD (C) spectra for **OPV3** in dodecane solution (4×10^{-5} M).

fluorescence characteristics of this trimer are blue shifted compared to **OPV4** and **OPV5** because of the decrease in conjugation length. When the temperature variable measurements in dodecane were performed with the same concentrations of **OPV3**, **OPV4**, and **OPV5**, the melting transition temperature for the stacks rises with conjugation length as a result of more $\pi-\pi$ interactions (see the Supporting Information). Change of solvent from pentane to heptane to dodecane has no systematic influence on the g_{abs} (7.2×10^{-3}, 7.3×10^{-3}, and 5.2×10^{-3}, respectively) at 6×10^{-6} M for **OPV4** at 283 K, suggesting similar types of aggregates in these solvents.

The melting of our stacks was further studied as function of concentration. The melting transition temperature drops with approximately 15 K for all **OPV** oligomers per decade of concentration as can be clearly deduced from the transition curves (Figure 3A−C). A linear dependence of the melting temperature with the *logarithmus naturalis* of the concentration was found (Figure 3D). Remarkably, this relationship is similar to that found for the melting of DNA, although DNA is a covalently linked system in an aqueous solution.[14] The thermodynamic parameters of the melting transition were evaluated from the van't Hoff plot (see the Supporting Information). The enthalpy decreased from $\Delta H = -129$ to -168 kJ mol^{-1} while the entropy decreased from $\Delta S = -335$ to -406 J mol^{-1} K^{-1} upon elongating the conjugation length from **OPV3** to **OPV5** (Table 1). The negative enthalpy and the entropy values illustrate that the aggregation is an enthalpy-driven process. The gain in enthalpy upon going to longer oligomers can be explained by more $\pi-\pi$ interactions existing in the aggregates. The growth in entropy could indicate that the organization in the stacks improves with the stacks of **OPV5** as the most well-defined.[15]

Small-Angle Neutron Scattering in Solution. SANS experiments were performed to elucidate the shape of the supramolecular aggregates in dilute solutions. In the present case, experiments were performed in d_{26}-dodecane with concentrations below 0.7 vol% for **OPV3** and **OPV4**, covering a range of scattering vectors from 0.03 nm^{-1} < Q < 3 nm^{-1}. In all cases, the variation of the scattering intensity $(d\Sigma/d\Omega)(Q)$ (normalized by the volume fraction ϕ) clearly indicated the presence of supramolecular assemblies. The scattering intensity from the solutions is described by $I(Q) = \varphi V_p P(Q) S(Q)$, where $P(Q)$ represents the form factor of the aggregates and $S(Q)$, a contribution due to interparticle correlations. For the dilute solutions considered in the present case, it is assumed that $S(Q) \approx 1$ (indicating negligible correlation effects), while $P(Q)$ was approximated by assuming an isotropic arrangement of cylindrical particles. Provided that the aspect ratio of the aggregates is large, i.e., $H \gg R$, the form factor contribution should reveal a broad region in which $I(Q) \approx Q^{-1}$. Moreover, if the dimensions of the cross section of the aggregates are rather well-defined, a secondary maximum at $Q \approx 4.49/R$ is expected at larger Q.

Indeed at low Q, the Holtzer plot representation of the scattering data clearly revealed an intensity decay $\propto Q^{-1}$, thus revealing the presence of cylindrical structures. Excellent fits

(14) For example, see: Marky, L. A.; Breslauer, K. J. *Biopolymers* **1987**, *26*, 1601−1620.

(15) This behavior is supported by the SANS data that show that the length of the rigid domains increases going from **OPV3** to **OPV4** (see SANS paragraph).

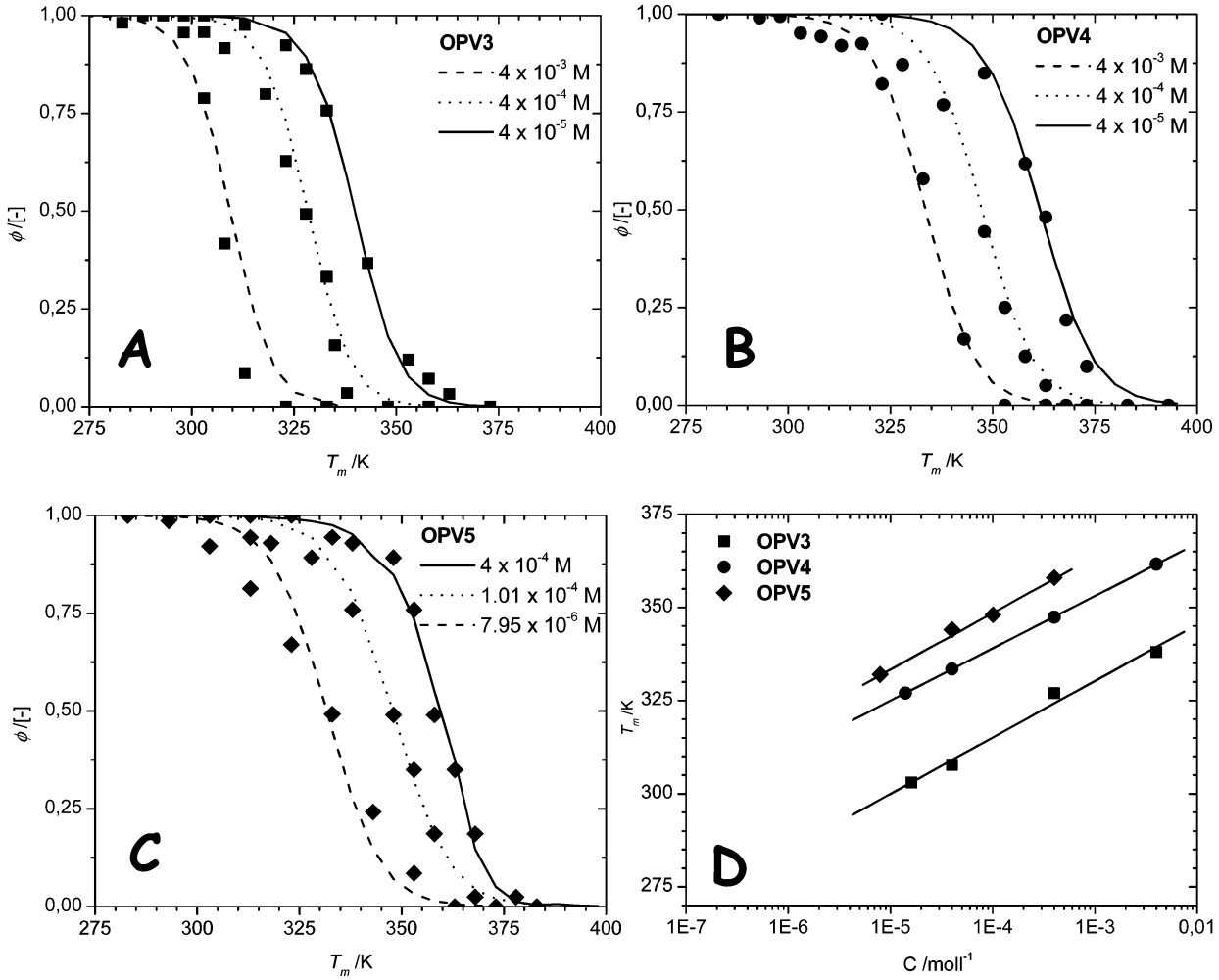

Figure 3. Plots of aggregated fraction (ϕ) versus temperature for **OPV3** (A), **OPV4** (B), and **OPV5** (C) with data points obtained from variable temperature CD measurements. Melting transition temperatures versus concentration showing a linear dependence for the oligomers (D).

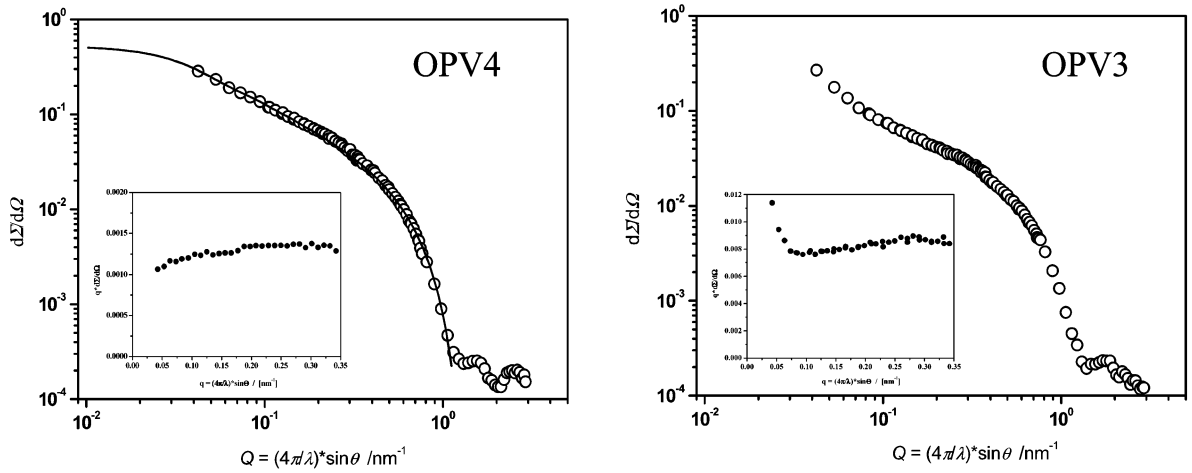

Figure 4. SANS intensity decay data versus Q from d_{26}-*n*-dodecane solutions containing **OPV4** (left) fitted according to a model assuming homogeneous cylindrical structures resulting in objects of height $L \approx 150$ nm and radius $R \approx 2.9$ nm. Inset shows the Holtzer plot representation of the data with a clear intensity decay $\propto Q^{-1}$. SANS intensity decay data versus Q from d_{26}-*n*-dodecane solutions containing **OPV3** (right) indicating the same type of structures as **OPV4**. Inset shows the Holtzer plot representation of the data with a clear intensity decay $\propto Q^{-1}$ at low Q and the deviation from the Q^{-1} behavior of the data at very low Q seemingly indicating intercolumnar interactions.

were based on a model assuming homogeneous rigid cylindrical structures, yielding columns with length $L \approx 150$ nm and a diameter of $D \approx 58$ Å for **OPV4** at $Q < 10$ nm^{-1} (Figure 4). It is assumed that the scattering intensity only reflects information on the form factor and thus the shape of the independent aggregates (see the Supporting Information). The **OPV3** SANS patterns can be interpreted by similar cylindrical structures. However, in this case, the deviation from the Q^{-1} behavior of the data at very low Q seems to indicate intercolumnar interactions, i.e., entanglements of the aggregates in a transient

network in which the crossing points are ~60 nm apart. This behavior is consistent with the results from rheological studies revealing a pronounced shear thinning effect due to alignment of highly anisotropic structures (see the Supporting Information). Dynamic oscillatory shear measurements show a fluidlike behavior for diluted solutions of **OPV3** at ambient temperature. At all frequencies is the $G' < G''$, whereas, at concentrated solutions, a crossover is observed at 6 rads^{-1}. In contrast, concentrated dodecane solutions of **OPV4** show a constant viscosity, nearly the solvent viscosity, which is an order of magnitude lower than that for **OPV3** at comparable concentrations, indicative of the absence of entanglements between the cylinders in solutions of **OPV4**. Evidently from the shifted side maximum of the form factor for **OPV3** (Figure 4), the diameter of the columns formed by **OPV3** ($D \approx 50$ Å) is smaller than those of **OPV4**, which is in agreement with the shorter π-system of the former compound. Molecular dynamics calculations reveal that the overall length of the **OPV4** hydrogen bonded dimer omitting the dodecyloxy tails is 57 Å and that of **OPV3** is 47 Å (Chart 1) corresponding well to the SANS data. This shows that the hydrogen bonded dimers stack on top of each other forming cylindrical structures. Similar scattering behavior was observed upon increasing the temperature indicating that height and diameter of the cylinders remain unchanged until 343 K when the scattered intensity for **OPV3** started to decrease strongly, signifying dissociation of the aggregates.[16]

So far, our studies in solution show that the OPV oligomers grow hierarchically, initially formed dimers by hydrogen bond formation that subsequently develop into stacks by $\pi-\pi$ interactions of the phenylenevinylenes with induced helicity via the chiral side chains (Figure 5).[17] The stack as a whole is still soluble in apolar solvents due to the long dodecyloxy side chains that are situated at the periphery of the aggregate. This hierarchical process shows that the information present at the molecular level, e.g., chiral side chains, long aliphatic chains, π-conjugated segments, and hydrogen bonding units, is expressed on the supramolecular level. The melting of the stacks depends on the concentration similar to that found for the denaturation of DNA in nature. The melting temperature and the persistence length of the stacks increase with elongation of the π-system of the OPV oligomers.

Tapping Mode Atomic Force Microscopy. The self-assembled stacks in heptane (6.7×10^{-6} M) were transferred to a solid support and investigated with tapping mode AFM. Numerous single fibers are found in cast films of **OPV4** on graphite (Figure 6). Although a constant width of about 40 nm for the fibers was found, the measured lateral dimensions are easily overestimated by a few tens of nanometers due to tip-convolution effects. Therefore, the values of the measured heights of the structures are a more accurate way to determine the diameter of the fibers, especially since soft tapping conditions were applied. The single cylindrical fibers of **OPV4** have

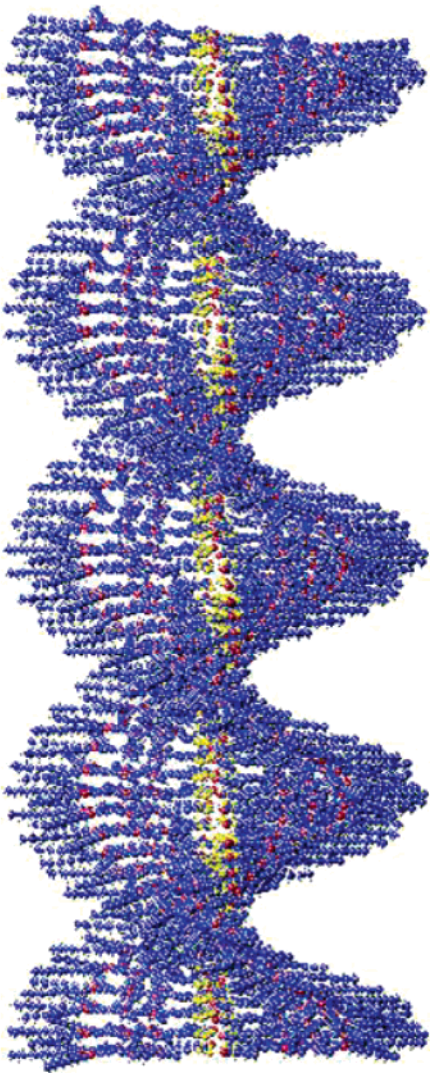

Figure 5. Self-assembled helical columnar architectures at low temperatures simulated for stacked **OPV4** dimers (Chart 1) with a distance between two adjacent hydrogen-bonded dimers of 0.35 nm, and the angle of rotation is close to 12° resulting in a pitch length of 6 nm.[17]

a uniform height of 52 Å, which corresponds very well to the SANS and MD calculations (Table 2).

In a few cases, two wires cross each other and the heights of these crossovers were about 96 Å as indicated from the line scan in Figure 6. The helicity of the stacks could not be observed. Helicity might still be present but not visible with AFM due to a pitch length that is too small or due to the achiral organization of the long aliphatic tails at the periphery of the stacks that mask the helicity of the interior of the stacks. The length of the **OPV4** fibers varies from 50 nm to 1 μm. Detailed analysis shows that the straight segments in the fibers have an average length of 125 nm (Figure 6). This persistence length fits very well with the length obtained by the SANS measurements (150 nm). Presumably, during the transfer process from solution to the solid support, the stacks present in solution self-assemble further in the stack direction to cylinders as long as 1 μm. This process is less defined resulting in kinks and a broad distribution of the length of the fibers.

The starting concentration of the drop cast solution is crucial for obtaining single fibers of **OPV4** on graphite (HOPG). When the solution was diluted to 1.3×10^{-6} M, a considerable amount

(16) Simultaneously, the ^{1}H NMR spectra of **OPV3** in d_{26}-*n*-dodecane at elevated temperature (388 K, see Supporting Information) revealed similar features as those in *d*-chloroform at room temperature. Cooling to 323 K gave rise to broadening of the signals of the aromatic protons indicating aggregation. At room temperature, extreme line broadening was observed.

(17) Preliminary quantum chemical calculations reveal that the distance between two adjacent hydrogen-bonded dimers is 0.35 nm and the angle of rotation is close to 12° resulting in a pitch length of 6 nm; Beljonne, D. Personal communication.

(18) Meijer, E. W.; Schenning, A. P. H. J. *Nature* **2002**, *319*, 353−354.

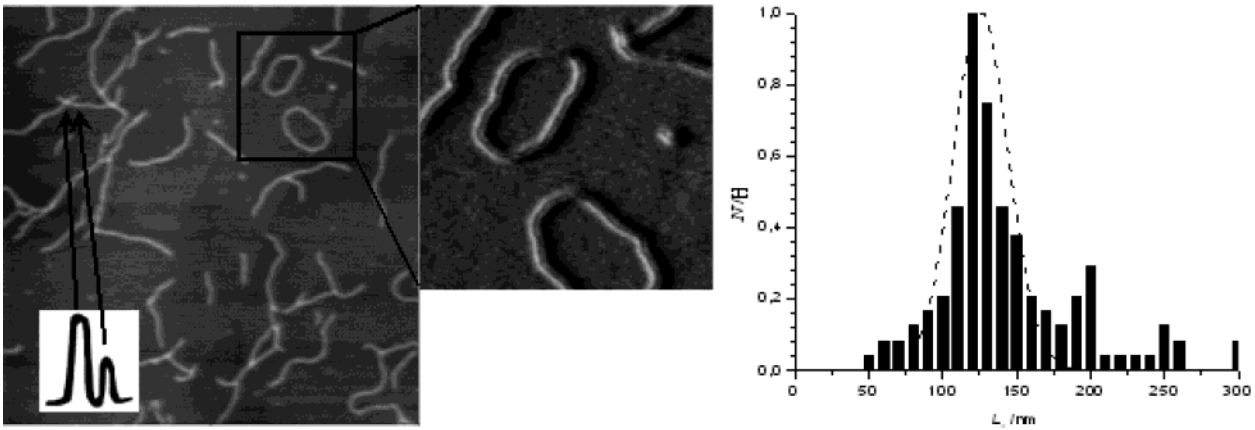

Figure 6. Tapping mode AFM images ($5 \times 5\ \mu m^2$) of **OPV4** on substrates drop cast from heptane solutions (6.7×10^{-6} M) on graphite (left). Inset shows two line scans over a crossover of two fibers and a single fiber for comparison, clearly the former (9.6 nm) being approximately double the latter (5.2 nm). From the indicated box area, the close-up phase image is shown (middle). Analysis (right) shows that straight segments of approximately 125 nm are present on the surface fitted by a Gaussian distribution function.

Table 2. Comparison of the Results of **OPV*n*** Determined by MD, Small-Angle Neutron Scattering (SANS), and Tapping Mode Atomic Force Microscopy (AFM)

length dimer	MD[a] (Å)	SANS[b] (Å)	AFM[c] (Å)
OPV3	47.0	50.1	47
OPV4	57.8	58.4	52
OPV5	68.6		58

[a] The dodecyloxy tails are omitted. [b] Determined from the position of the side maximum of the Bessel function. [c] Deduced from height profiles.

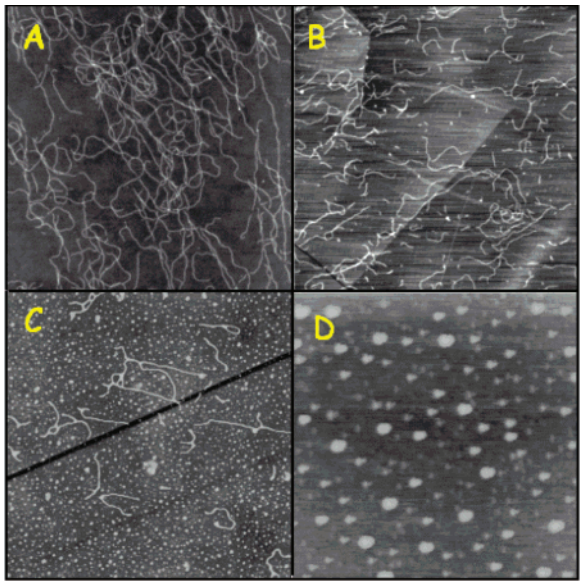

Figure 7. Tapping mode AFM images of **OPV4** on graphite showing different types of aggregation on the surface depending on the concentration of the drop cast solution: 1.3×10^{-4} M, $10 \times 10\ \mu m^2$ (A); 1.3×10^{-5} M, $7 \times 7\ \mu m^2$ (B); 1.3×10^{-6} M, $7 \times 7\ \mu m^2$ (C); and 1.3×10^{-7} M, $7 \times 7\ \mu m^2$ (D).

of globular structures next to the self-assembled single nanowires was visible (Figure 7C). The formation of globular structures during the casting procedure is probably the outcome of uncontrolled self-assembly of the molecularly dissolved fractions, which are already present in solution at this concentration (Figure 3). Further dilution to 1.3×10^{-7} M showed only globular structures (Figure 7D). At this concentration, optical spectroscopy showed that only molecular dissolved species are present in solution at room temperature (Figure 3D). Applying a more concentrated solution of 1.3×10^{-4} M resulted in a highly intertwined network of merging individual strands on the surface (Figure 7A). Similar observations were obtained for **OPV3** and **OPV5** (see Supporting Information). In the case of **OPV3**, however, all concentrations at which the objects on the surface change from globular shape to isolated wires and fibrillar networks are higher, while, in the case of **OPV5**, these concentrations are lower. This behavior corresponds very well with the behavior in solution where the stability of the stacks increases with the conjugation length. Apparently, and striking at first glance, is the requirement to first form stacks in solution before casting this solution to a surface to obtain fibers at graphite. Although evaporation of the solvent leads to an increase of the concentration, molecule−graphite interactions can be dominant over the formation of stacks starting off from too diluted solutions. The results show the subtleties of transferring supramolecular assemblies to surfaces.

The deposition of our stacks (6.7×10^{-6} M in heptane) was also investigated on different types of solid support. On pretreated silicon oxide wafers, single fibers were obtained similar to the behavior on graphite (see Supporting Information). Lamellar clusters of stacks of **OPV4** were formed on polar glass slides (Figure 8). Here, the width of the fibers varies largely while the height is in all cases approximately 5 nm. On mica, the same result was found as that for glass (see the Supporting Information). Graphite and silicon oxide wafers are more hydrophobic surfaces resulting in single cylindrical fibers, while, on glass and mica, which are more hydrophilic, a lamellar structure exists. The latter can probably be ascribed to more favorable mutual interactions of the stacks rather than those between the stacks and the surface. When the glass substrate was coated with a thin layer of carbon, similar results are obtained as those on graphite, illustrating that it is possible to suppress repulsive surface interactions toward the stacks (see the Supporting Information). Applying a droplet of the same solution to gold surfaces resulted in a complete destruction of the stacks (Figure 8). Presumably the molecule−gold interactions are so strong that they overrule the molecule−molecule interaction within the stacks resulting in ill-defined globular objects.

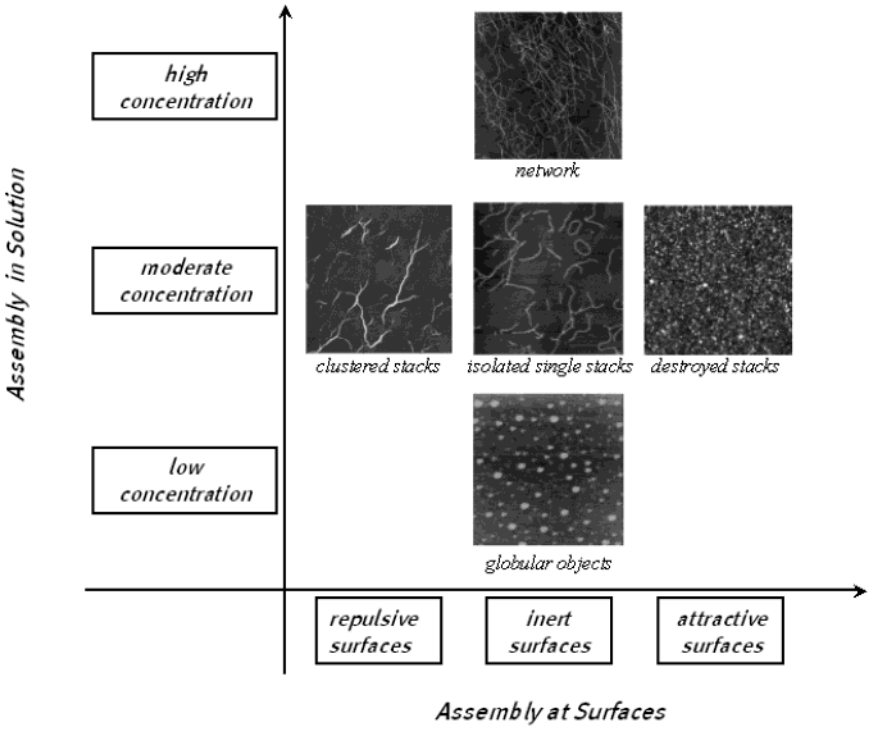

Figure 8. Plot representing the role of the interaction of the surface toward the stacks versus the concentration in the transfer process of the supramolecular stacks formed in solution to the solid state. Tapping mode AFM images ($7 \times 7\ \mu m^2$) of **OPV4** (6.7×10^{-5} M), glass (repulsive surface), graphite (inert surface, three concentrations), and gold (attractive surface).

The observations described above stunningly illustrate the importance that the molecule−surface interactions are crucial to successfully transfer the supramolecular stack present in solution to a solid support (inert surfaces, Figure 8). When the molecule−molecule interactions present in the supramolecular stacks in solution are perturbed by stronger molecule−surface interactions (attractive surfaces), the stacks cannot be transferred to the surface. Repulsive surfaces give rise to clustering of stacks due to the minimization of the contact area between the stack and the support resulting in lamellar arrays of stacks (Figure 8). Together with the fact that the concentration and the temperature of the cast solution determines the equilibrium between individual molecules and the supramolecular stack, it is obvious that many variables control the successful transfer of stacks from solution to surfaces. However, comprehensive knowledge of all intermolecular interactions gives rise to controlled transfer of π-conjugated assemblies to specific surfaces.

Conclusion

Photophysical measurements show that it is possible to self-assemble π-conjugated molecules into helical stacks in solution similar to processes found in nature. SANS measurements reveal that rigid cylindrical objects are formed of 150 nm in length with a diameter of 6 nm for **OPV4**. Temperature and concentration variable measurements show that the stability of the stacks in solution increases with the conjugation length as a result of more π−π interactions. The transfer of the supramolecular stacks from solution to a solid support is a very delicate process. Only if specific concentrations and specific solid supports are chosen, isolated cylinders are observed. Upon transfer of the stacks to the surface, the stacks tend to grow and form kinks on the surface in a less controlled manner. The transfer of these self-assembled fibers is one of the first examples of single organic fibers consisting of self-assembled chromophores on a solid support. The strategy to construct individual nanosized columns might be interesting in the field of supramolecular electronics.[18] The design of such nanodevices must be such that all components behave as an inert surface toward self-assembled stacks.

Acknowledgment. La Laboratoire Léon Brillouin (J. Teixeira, CEA Saclay, France) is gratefully acknowledged for the beamtime using the small-angle diffractometer PAXE located at the ORPHEE reactor. Xianwen Lou and Joost van Dongen are acknowledged for MALDI-TOF measurements, and Henk Eding is acknowledged for elemental analysis. This research was supported by The Netherlands Organization for Scientific Research (NWO), the Royal Dutch Academy for Arts and Sciences (KNAW), and DSM.

Supporting Information Available: Synthetic procedures, a description of the photophysical apparatus, procedures followed during the atomic force microscopy, and neutron scattering measurements. NMR spectra (^{1}H NMR, ^{13}C NMR, ^{1}H−^{1}H COSY, ^{1}J HETCOR and ^{3}J HETCOR) and its full assignment for **OPV4T**. UV−vis and fluorescence data for **OPVn** in chloroform solutions. CD spectra for **OPVn** in dodecane at 4×10^{-4} M, the van 't Hoff plot, and the variable temperature ^{1}H NMR in dodecane. The graphs of the dynamic oscillatory shear experiments are given. AFM images of **OPV4** on silicon oxide wafers, mica, and carbon coated glass as well as the AFM images of **OPV3**, **OPV4**, and **OPV5** at 6.7×10^{-6} M. This material is available free of charge via the Internet at http://pubs.acs.org.

JA0383118